



## A Catalytic Reduction of 4-Nitrophenol Utilizing Bimetallic CuO-Co<sub>3</sub>O<sub>4</sub> Nanoparticles Synthesized via *Wrightia tinctoria* Extract: A Green Approach

M. JEEVARATHINAM<sup>b</sup>, ABHISHIKTA HALDER<sup>b</sup>, ARCHANA MANOJ<sup>b</sup> and I.V. ASHARANI<sup>\*a</sup>

Department of Chemistry, School of Advanced Sciences, Vellore Institute of Technology, Vellore-632014, India

\*Corresponding author: E-mail: asharani.iv@vit.ac.in

Received: 14 February 2024;

Accepted: 4 April 2024;

Published online: 30 April 2024;

AJC-21623

In this investigation, copper oxide (CuO), cobalt oxide (Co<sub>3</sub>O<sub>4</sub>) and bimetallic copper oxide-cobalt oxide (CuO-Co<sub>3</sub>O<sub>4</sub>) nanoparticles were synthesized using an aqueous extract of *Wrightia tinctoria* leaves and characterized through UV-Vis, FT-IR, XRD, TEM and zeta potential analyses. The FT-IR analysis identified that specific phytoconstituents are responsible for the reduction and capping agents in nanoparticle synthesis. TEM analysis determined size and shape and zeta potential analysis assessed stability. The CuO and Co<sub>3</sub>O<sub>4</sub> NPs, synthesized through an eco-friendly approach, were employed for 4-nitrophenol reduction with sodium borohydride. The reaction rate, was computed at  $1 \times 10^{-4} \text{ s}^{-1}$ , which indicated the pseudo-first-order kinetics. The synthesis of 4-aminophenol was also successfully achieved demonstrated that the excellent catalytic activity of CuO, Co<sub>3</sub>O<sub>4</sub> and CuO-Co<sub>3</sub>O<sub>4</sub> nanoparticles as catalysts.

**Keywords:** Bimetallic nanoparticles, Catalytic activity, Zeta potential, 4-Nitrophenol reduction.

### INTRODUCTION

Study in nanoscience and nanotechnology has become a significant area of finding applications in water pollution, sensors, medical sciences and engineering [1-4]. Analysts expect these advancements to impact various industries influencing the environment [5]. Nanoparticles, a distinct class of materials, exhibit unique characteristics compared to their bulk and molecular counterparts [6,7]. The catalytic, optical, physico-chemical, electronic and photocatalytic properties depend on surface morphology, shape and size [8-10]. Creating multicomponent and multifunctional metal nanomaterials involves combining different metal precursors to form nanoalloys with advanced properties [11-13]. Whether bimetallic or trimetallic, these nanomaterials show distinctive and improved properties compared to their monometallic counterparts, benefiting from the synergistic effects of different elements [14-17].

Modifying the chemical compositions and structural morphologies of multi-metallic nanoparticles allows precise manipulation of their key properties, particularly in catalytic and optical efficiency. This adaptability expands their applications across various scientific and technological fields, including catalysis, sensing and medical applications [18-20]. Notably,

copper and cobalt-based nanoparticles have gained recognition for their effectiveness in catalysis, printed electronics, sensors and various applications [21-23]. Recent studies also highlight the superior antibacterial properties of copper and cobalt-based nanoparticles compared to other metal nanoparticles [24,25].

Metallic nanoparticles synthesis can be achieved through either chemical or biological methods. While chemical methods are effective, concerns arise due to the use of toxic chemicals absorbed on nanoparticle surfaces, potentially causing adverse effects. In contrast, biogenic synthesis methods involving microorganisms, enzymes, fungi and plant extracts offer an environmentally friendly alternative. Therefore, the eco-friendly biogenic synthesis of CuO-Co<sub>3</sub>O<sub>4</sub> nanoparticles emerges as a sustainable approach [26,27]. The properties of metal oxide nanoparticles in plant extract-mediated synthesis are directly influenced by a number of experimental factors, such as temperature, reaction duration and the mass ratio between the extract and metal salt [28,29].

*Wrightia tinctoria* (WT), a deciduous tree native to Burma and India with light gray bark, belongs to the Apocynaceae family. The analysis of *W. tinctoria* leaf extract has revealed the presence of phenolic compounds, especially flavonoids, known for their antioxidant properties essential in effective

scavenging and nanoparticle production due to their ability to donate hydrogen and specific structural characteristics [30].

Current concerns about water contamination affecting surface and groundwater have arisen due to its adverse health effects [31-33]. The main reason for this problem is the excessive concentration of harmful and persistent pollutants, especially 4-nitrophenol [34-36]. 4-Nitrophenol is extensively used in industries like pharmaceuticals and textiles for producing herbicides, insecticides, corrosion inhibitors, synthetic dyes, paints and pH indicators [37-40]. Consequently, the 4-nitrophenol reduction to 4-aminophenol has become crucial due to the lower toxicity of 4-aminophenol [36,41].

In this investigation, the primary focus is on the eco-friendly synthesis of bimetallic CuO-Co<sub>3</sub>O<sub>4</sub> nanoparticles from *Wrightia tinctoria* leaves extract and applied for the catalytic conversion of 4-nitrophenol into 4-aminophenol in the presence of sodium borohydride (NaBH<sub>4</sub>).

## EXPERIMENTAL

Cobalt sulphate heptahydrate (CoSO<sub>4</sub>·7H<sub>2</sub>O) and copper sulphate pentahydrate (CuSO<sub>4</sub>·5H<sub>2</sub>O) were obtained from Sisco Research Laboratory, India. Sodium hydroxide (NaOH) was sourced from Molychem and 4-nitrophenol was acquired from Avra Chemical Pvt. Ltd. Sodium borohydride (NaBH<sub>4</sub>) and ninhydrin (C<sub>9</sub>H<sub>6</sub>O<sub>4</sub>) were purchased from SRL Chemical Pvt. Ltd. Without further additional purification, all the reagents employed in this investigation were of analytical grade. The preparation of all solutions was done using double-distilled water.

**Preparation of *Wrightia tinctoria* leaf extract:** Fresh and nutrient-rich leaves of *Wrightia tinctoria* plant were locally sourced in Thrissur city, India. These leaves were carefully washed with double-distilled water to eliminate any dust or contaminants. Subsequently, they were preserved in a air-dried dark environment at room temperature for 7 days. Once fully dried, the leaves were finely grounded to powder and stored. For the extraction process, 10 g of powdered leaves were boiled in 200 mL of double-distilled water for 3 h at 80 °C and then filtered. The resulting filtrate was refrigerated for further use.

**Synthesis of CuO-Co<sub>3</sub>O<sub>4</sub> bimetallic nanoparticles:** To obtain CuO-Co<sub>3</sub>O<sub>4</sub> bimetallic NPs, the first step involved the synthesis of CuO nanoparticles. This process commenced by dissolving 2.416 g of CuSO<sub>4</sub>·5H<sub>2</sub>O in 80 mL of water. The solution underwent heating to 80 °C within an oil bath while being consistently stirred. Subsequently, 20 mL of *W. tinctoria* leaf extract was gradually introduced into the reaction mixture. By alkalizing the mixture with NaOH to adjust its pH, the solution experienced a change in colour from green to brown within 2 h, indicating the successful formation of CuO nanoparticles. The resulting mixture was centrifuged and the precipitate was washed thoroughly with deionized water followed by ethanol to eliminate impurities and finally dried at 80 °C. Following a similar approach, cobalt oxide (Co<sub>3</sub>O<sub>4</sub>) nanoparticles were also synthesized using CoSO<sub>4</sub>·7H<sub>2</sub>O precursor (2.78 g). After synthesizing CuO and Co<sub>3</sub>O<sub>4</sub> nanoparticles independently, they were combined in a 1:1 weight ratio and ground together in a mortar. The mixture was then subjected to calcin-

ation at 700 °C for 2 h to obtain CuO-Co<sub>3</sub>O<sub>4</sub> bimetallic nanoparticles (BMNPs).

**Characterization:** FTIR spectroscopy, utilizing the Shimadzu IR Affinity-1 instrument, was employed to analyze the functional groups existing within the aqueous leaf extract. The UV-visible spectra (JASCO V-670 PC) were employed to monitor the reduction of 4-nitrophenol. The XRD analysis (BRUKER D8) using CuK $\alpha$  radiation ( $\lambda = 1.5406 \text{ \AA}$ ) scanned  $2\theta$  from 20 to 90°, providing insights into the crystal structure and size of the metal oxide nanoparticles. The zeta potential analysis (Horiba Scientific SZ-100) was conducted to evaluate the stability of the synthesized nanoparticles. Additionally, the high-resolution transmission electron microscopy (HR-TEM) (FEI-Tecna G2 20 Twin) were utilized to examine the surface size and structure of CuO-Co<sub>3</sub>O<sub>4</sub> BMNPs.

**Catalytic reduction of 4-nitrophenol :** To investigate the catalytic efficacy of the synthesized CuO, Co<sub>3</sub>O<sub>4</sub> and CuO-Co<sub>3</sub>O<sub>4</sub> BMNPs, the reduction of 4-nitrophenol at  $1 \times 10^{-4} \text{ M}$  was conducted using NaBH<sub>4</sub> ( $5 \times 10^{-3} \text{ M}$ ) as reducing agent. The progress of the reduction reaction was observed using a UV-visible spectrophotometer. Additionally, the impact of NaBH<sub>4</sub> concentration and catalyst dosage on the catalytic reduction was also investigated. The correlation between time and the logarithm of the ratio of concentration to initial concentration [ $\ln(C/C_0)$ ] was analyzed to determine the kinetics of the reaction.

## RESULTS AND DISCUSSION

**UV-visible studies:** The absorbance peaks at 264 and 329 nm in the UV-Vis spectrum (Fig. 1) of the aqueous *W. tinctoria* leaf extract indicate the existence of polyphenolic alcohol groups [42], which are responsible for reducing the metal ions and contributing to the formation of metal/metal oxide nanoparticles.

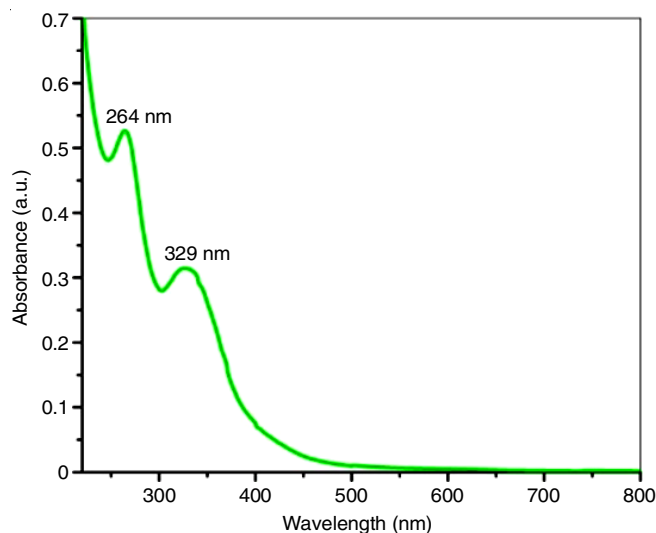


Fig. 1. UV-vis spectrum of *Wrightia tinctoria* leaves extract

**Zeta potential studies:** The electrostatic self-assembly of CuO-Co<sub>3</sub>O<sub>4</sub> bimetallic nanoparticles and their stability were performed through zeta potential analysis. As shown in Fig. 2, the zeta potential values were determined to be -24.2 mV for

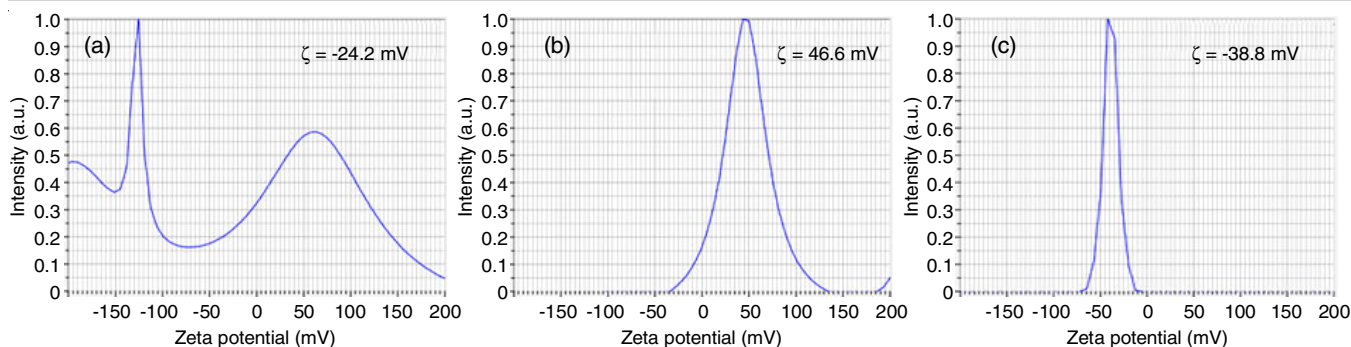


Fig. 2. Zeta potential analysis of (a) CuO nanoparticles, (b) Co<sub>3</sub>O<sub>4</sub> nanoparticles, and (c) CuO-Co<sub>3</sub>O<sub>4</sub> bimetallic nanoparticles

CuO nanoparticles and 46.6 mV for Co<sub>3</sub>O<sub>4</sub> nanoparticles. The negative zeta potential of CuO nanoparticles could facilitate the electrostatic attraction of Co<sub>3</sub>O<sub>4</sub> [43]. The zeta value for CuO-Co<sub>3</sub>O<sub>4</sub> bimetallic nanoparticles was found to be -38.8 mV. These zeta potential values suggest that the nanoparticles tend to uphold dispersion and resist aggregation, mainly due to the presence of electrical repulsion forces [44]. The negative zeta values indicate the overall stability of the prepared CuO-Co<sub>3</sub>O<sub>4</sub> bimetallic nanoparticles.

**FT-IR studies:** Fig. 3 depicts the FT-IR spectra of *W. tinctoria* extract, CuO, Co<sub>3</sub>O<sub>4</sub> and CuO-Co<sub>3</sub>O<sub>4</sub> bimetallic nanoparticles. Within the *W. tinctoria* spectrum, the peaks at 3304, 2100, 1635 and 710 cm<sup>-1</sup> correspond to -OH, C=N, N-H and C-H stretching vibrations, respectively, signify the existence of functional groups in the phytoconstituents of *W. tinctoria* extract. In Fig. 3b-d, the peaks observed in the synthesized metal oxides at 1074 cm<sup>-1</sup> suggest the C-O stretching and the peak at 600-400 cm<sup>-1</sup> indicates the formation of metal-oxygen (M-O) bonds, providing evidence for the successful synthesis of CuO-Co<sub>3</sub>O<sub>4</sub> bimetallic nanoparticles [45,46].

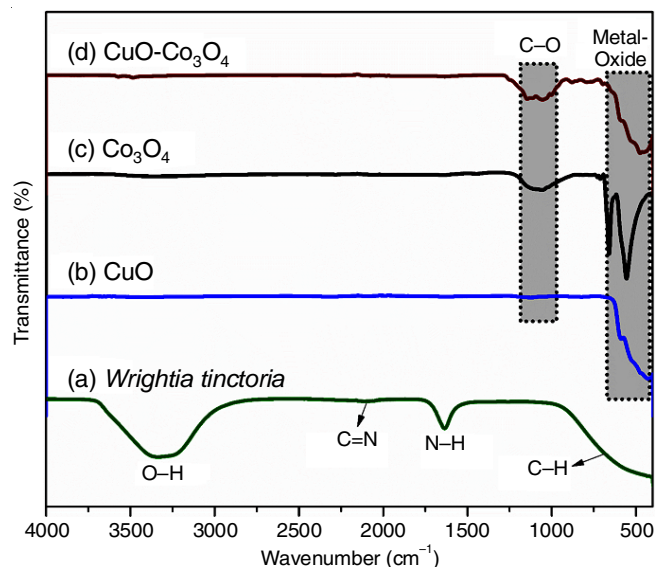


Fig. 3. FT-IR spectra of (a) aqueous extract of *W. tinctoria*, (b) CuO NPs, (c) Co<sub>3</sub>O<sub>4</sub> NPs and (d) CuO-Co<sub>3</sub>O<sub>4</sub> bimetallic NPs

**XRD studies:** The Co<sub>3</sub>O<sub>4</sub> nanoparticles exhibit the distinct peaks at 2 $\theta$  angles of 30.1°, 38.5°, 38.2°, 44.6°, 59.4°, 65.3°, corresponding to (220), (311), (222), (400), (511) and (440)

crystalline planes, respectively, confirming the pristine cubic phase according to JCPDS card No. 76-1802 [47]. For CuO nanoparticles, the peaks at 2 $\theta$  angles of 32.5°, 35.4°, 38.7°, 48.7°, 53.4°, 58.3°, 61.5°, 65.8°, 72.4° and 74.8° identified as (110), (002), (111), ( $\bar{2}$ 02), (020), ( $\bar{1}$ 13), (202), (022), (311) and (004), respectively, validate the monoclinic structure of CuO nanoparticles (JCPDS card No. 05-0661) [48]. In case of bimetallic nanoparticles, the 2 $\theta$  angles diffraction peaks for CuO and Co<sub>3</sub>O<sub>4</sub> confirm the monoclinic structure of CuO and the cubic structure of Co<sub>3</sub>O<sub>4</sub> in the bimetallic nanoparticles (Fig. 4). Using Scherrer's equation (eqn. 1), an average crystallite size of 21.4, 13.8 and 20.4 nm for CuO, Co<sub>3</sub>O<sub>4</sub> and CuO-Co<sub>3</sub>O<sub>4</sub> bimetallic nanoparticles was determined.

$$D = \frac{k\lambda}{\beta \cos \theta} \quad (1)$$

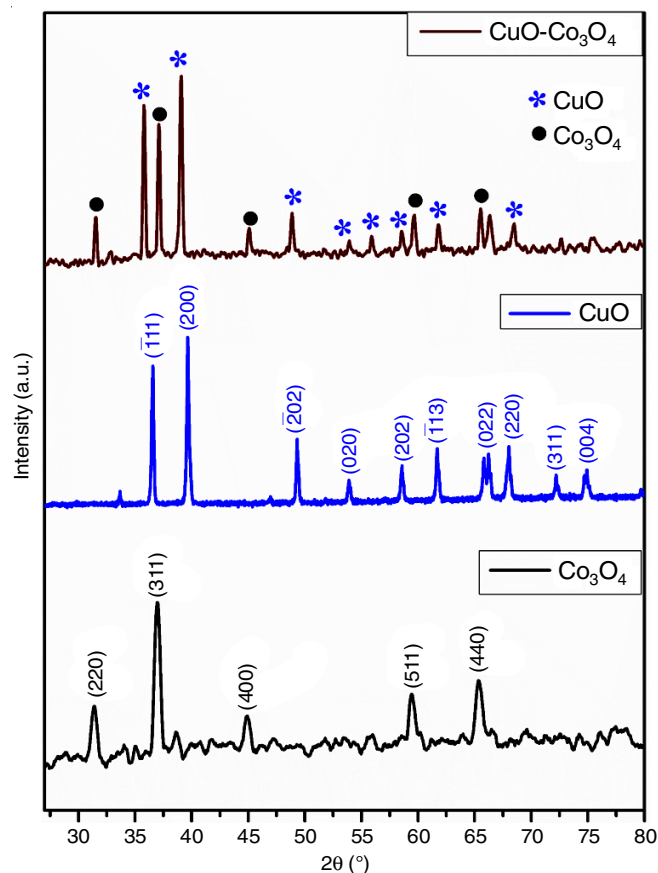


Fig. 4. P-XRD spectra of Co<sub>3</sub>O<sub>4</sub> NPs, CuO NPs and CuO-Co<sub>3</sub>O<sub>4</sub> bimetallic NPs

where  $D$  represents the average crystalline size,  $\lambda$  is the X-ray wavelength (nm),  $\beta$  is the full width at half maximum (FWHM) and  $\theta$  is the Bragg's angle of diffraction.

**TEM studies:** The TEM images (Fig. 5a-b) demonstrate the uniform dispersion of spherical CuO-Co<sub>3</sub>O<sub>4</sub> bimetallic nanoparticles, synthesized using a green method. All particles were observed within the 100 nm range and the analysis of the TEM image's histogram distribution curve *via* Image J software revealed an average particle size of 26 nm as depicted in Fig. 5d. The SAED pattern illustrated in Fig. 5c demonstrates the exceptional crystalline quality of the prepared bimetallic nanoparticles, characterized by clear spots and ring patterns.

**BET analysis:** BET study has been employed for the surface analysis and its characteristics of CuO-Co<sub>3</sub>O<sub>4</sub> bimetallic nano-

particles by the reactional N<sub>2</sub> adsorption-desorption method. The crucial role in controlling the primary aspect of catalytic activity is performed by the direct adsorption of organic compounds onto the catalyst plane. Fig. 6 exhibited the adsorption-desorption isotherm of nitrogen for the prepared bimetallic nanoparticles. It showed the type-IV isotherm with narrow adsorption-desorption of H3-type hysteresis loops (Fig. 6). The surface area of CuO-Co<sub>3</sub>O<sub>4</sub> bimetallic nanoparticles was found to be 48.609 m<sup>2</sup>/g. The porosity has been determined from the Barrett-Joyner-Halenda (BJH) relation and found to be 3.058 nm, which indicates the pores are mesoporous. Therefore, these specific surface area results of CuO-Co<sub>3</sub>O<sub>4</sub> bimetallic nanoparticles could show the higher catalytic activity in the reduction of 4-nitrophenol to 4-aminophenol.

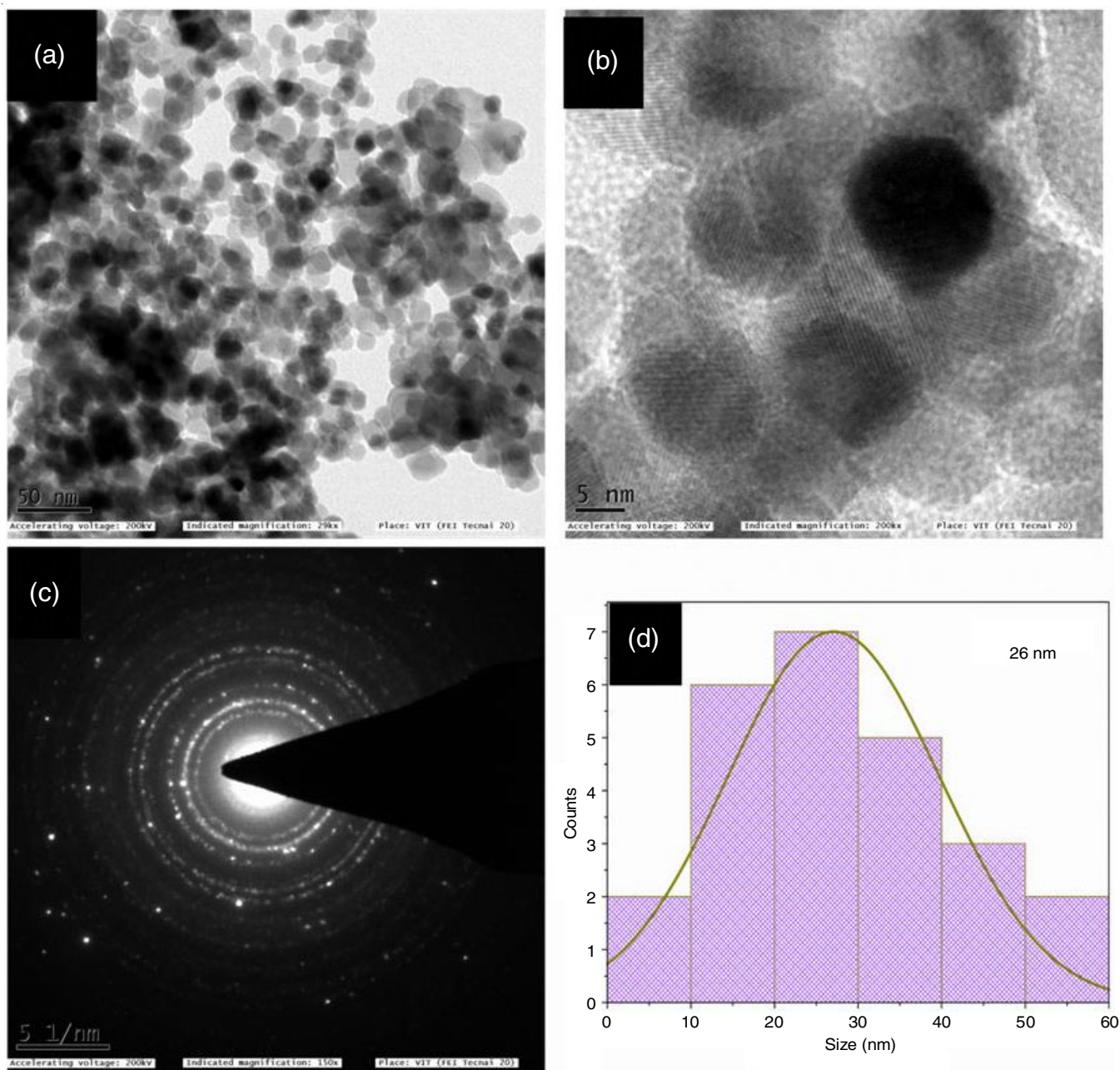
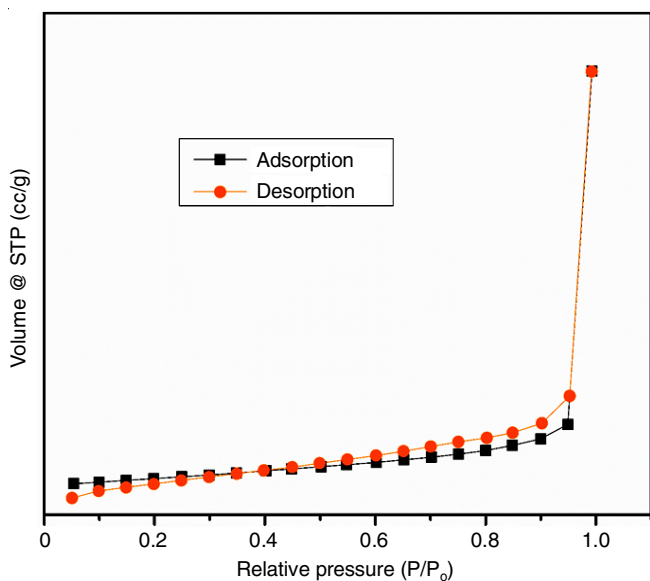


Fig. 5. (a,b) TEM images of synthesized CuO-Co<sub>3</sub>O<sub>4</sub> bimetallic nanoparticles from *Wrightia tinctoria*, (c) SAED pattern of bimetallic nanoparticles and (d) Histogram distribution curve

Fig. 6. N<sub>2</sub> adsorption-desorption graph of CuO-Co<sub>3</sub>O<sub>4</sub> bimetallic nanoparticles

**Catalytic reduction of 4-nitrophenol:** The reduction reaction of 4-nitrophenol ( $1 \times 10^{-4}$  M) to 4-aminophenol was carried out by using NaBH<sub>4</sub> ( $5 \times 10^{-3}$  M) to evaluate the catalytic efficiency of prepared CuO-Co<sub>3</sub>O<sub>4</sub> bimetallic nanoparticles (1 mg/mL). Initially, the characteristic peak of 4-nitrophenol was detected at 317 nm. Upon the introduction of NaBH<sub>4</sub>, this peak shifted to 400 nm, indicating the formation of 4-nitrophenolate ion. In the absence of catalyst, the absorbance intensity at 400 nm remained constant for 24 h. However, introducing a catalyst resulted in a significant reduction in absorbance intensity at 400 nm. In addition to this, a new peak appeared at 300 nm, which indicated the formation of 4-aminophenol. The rate of the reaction was computed to be  $1 \times 10^{-4}$  s<sup>-1</sup>. Similarly, the rate of the reaction for monometallic CuO and Co<sub>3</sub>O<sub>4</sub> was found to be 0.87 and  $0.78 \times 10^{-4}$  s<sup>-1</sup>, respectively.

**Effect of different parameters on reduction of 4-nitrophenol:** Studies of 4-nitrophenol reduction involved exploring the influence of varying CuO-Co<sub>3</sub>O<sub>4</sub> catalyst dosage and NaBH<sub>4</sub> concentration. The reaction rate, determined to adhere to pseudo-first-order kinetics, is visually represented in Fig. 7. Significantly, the optimal reaction rate was attained at a catalyst dosage of 1 mg/mL and at  $5 \times 10^{-3}$  M NaBH<sub>4</sub> concentration. This increased rate can be attributed to the increased availability of active sites, facilitating a more efficient reduction with a greater catalyst dosage. Moreover, the higher NaBH<sub>4</sub> concentration supports electron transfer between the nitro group and NaBH<sub>4</sub>. Consistently, the reaction exhibited pseudo-first-order kinetics and the relevant rate constant values are shown in Table-1.

**Confirmation of reduction product:** To confirm the reduction product, 4-aminophenol was individually extracted from the reaction mixture using ethyl acetate. Subsequently, the <sup>1</sup>H NMR spectra of the extracted samples were recorded to confirm the formation of 4-aminophenol. In the <sup>1</sup>H NMR spectra (Fig. 8) of 4-aminophenol, the peaks were observed at δ (ppm): 8.35 (s, 1H)-OH proton, 6.49-6.41 (q, 4H)-aromatic proton, 4.37 (s, 2H)-NH<sub>2</sub> proton. The obtained results are also consistent with the previous reports [49,50].

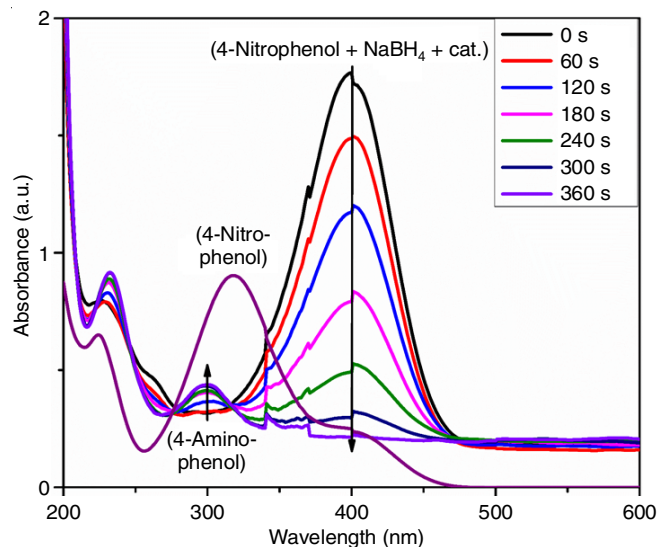
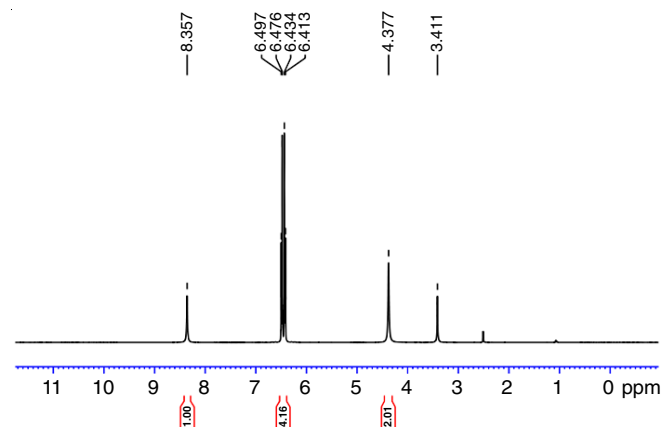
Fig. 7. The UV absorption spectra of catalytic reduction of 4-aminophenol using CuO-Co<sub>3</sub>O<sub>4</sub> bimetallic nanoparticles

TABLE-1  
CATALYTIC REDUCTION OF 4-NITROPHENOL ( $1 \times 10^{-4}$ ) TO 4-AMINOPHENOL WITH DIFFERENT PARAMETERS AND THEIR RATE CONSTANT VALUES

Catalyst dosage (mg/mL)	Conc. of NaBH <sub>4</sub> ( $\times 10^{-3}$ M)	Rate constant (k) $\times 10^{-4}$ s <sup>-1</sup>
1.00	5.00	1.00
1.00	2.50	0.94
1.00	1.25	0.68
0.50	5.00	0.66
0.25	5.00	0.68

Fig. 8. <sup>1</sup>H NMR spectra of 4-aminophenol

**Recyclability and stability of CuO-Co<sub>3</sub>O<sub>4</sub> bimetallic nanoparticles:** The study also explored the stability and reusability of the CuO-Co<sub>3</sub>O<sub>4</sub> bimetallic nanoparticles. The catalyst underwent separation using centrifugation and thorough washing with deionized water and ethanol. Subsequent reduction reactions were performed over four cycles using the recovered catalyst. Following the fourth cycle, a slight decrease in the conversion percentage from 88.99% to 85.02% was observed, indicating the sustained catalytic efficiency of CuO-Co<sub>3</sub>O<sub>4</sub> bimetallic nanoparticles (Fig. 9a). The XRD analysis was also conducted to assess the stability of the recycled CuO-Co<sub>3</sub>O<sub>4</sub> bimetallic nano-

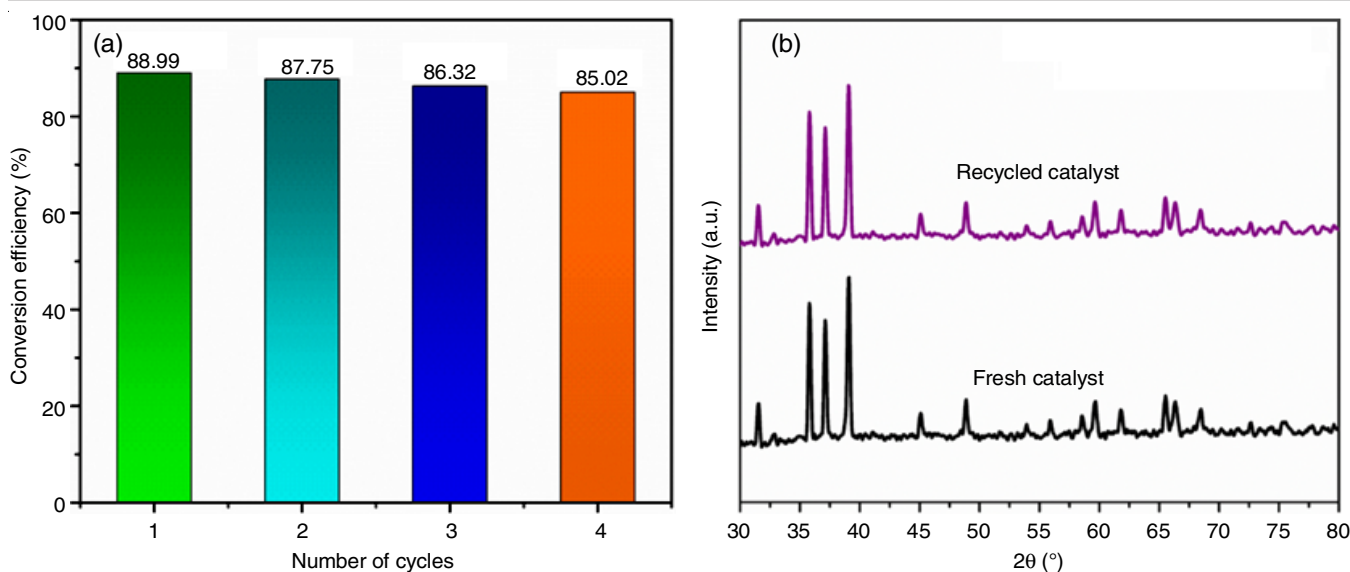


Fig. 9. Recyclability of CuO-Co<sub>3</sub>O<sub>4</sub> bimetallic nanoparticles

particles (Fig. 9b). The findings showed no change in the peak position of 2θ, suggesting that CuO-Co<sub>3</sub>O<sub>4</sub> BMNPs synthesized via *Wrightia tinctoria* mediated green synthesis exhibit notable stability and reusability.

### Conclusion

In this work, mono and bimetallic nanoparticles *viz.* Co<sub>3</sub>O<sub>4</sub> nanoparticles, CuO nanoparticles and CuO-Co<sub>3</sub>O<sub>4</sub> bimetallic nanoparticles utilizing an aqueous extract sourced from *Wrightia tinctoria*. The dual role of plant extract acted as capping and reducing agent was confirmed through FT-IR spectral analysis. The stability of the synthesized catalysts was indicated by zeta potential measurements. The TEM images unveiled that the CuO-Co<sub>3</sub>O<sub>4</sub> bimetallic nanoparticles exhibit a spherical morphology with an average particle size of 26 nm. The catalytic activity of the synthesized catalyst exhibited a rate constant of  $1 \times 10^{-4} \text{ s}^{-1}$  for CuO-Co<sub>3</sub>O<sub>4</sub> bimetallic nanoparticles, surpassing that of monometallic CuO and Co<sub>3</sub>O<sub>4</sub> nanoparticles. The prepared bimetallic nanoparticles (CuO-Co<sub>3</sub>O<sub>4</sub>) display potential as a versatile catalyst for both environmental pollutant remediation and the organic transformation reactions.

### ACKNOWLEDGEMENTS

The study was facilitated by the VIT SEED Grant-RGEMS Fund (SG20220085) from Vellore Institute of Technology, Vellore, India.

### CONFLICT OF INTEREST

The authors declare that there is no conflict of interests regarding the publication of this article.

### REFERENCES

- D. Ling, M.J. Hackett and T. Hyeon, *Nano Today*, **9**, 457 (2014); <https://doi.org/10.1016/j.nantod.2014.06.005>
- J. Zheng, M.S. Stevenson, R.S. Hikida and P.G. Van Patten, *J. Phys. Chem. B*, **106**, 1252 (2002); <https://doi.org/10.1021/jp013108p>
- V.A. Bharathan, V. Yadukiran, A. Lazar, A.P. Singh and C.P. Vinod, *ChemistrySelect*, **1**, 140 (2016); <https://doi.org/10.1002/slct.201500006>
- H. Karimi-Maleh, F. Karimi, S. Malekmohammadi, N. Zakariae, N. Atar, R. Esmaceli, S. Rostammia, M.L. Yola, S. Movaghgharnezhad, S. Rajendran, A. Razmjou, Y. Orooji, S. Agarwal and V.K. Gupta, *J. Mol. Liq.*, **310**, 113185 (2020); <https://doi.org/10.1016/j.molliq.2020.113185>
- C. Huang, A. Notten and N. Rasters, *J. Technol. Transf.*, **36**, 145 (2011); <https://doi.org/10.1007/s10961-009-9149-8>
- P. Biswas and C.-Y. Wu, *J. Air Waste Manage. Assoc.*, **55**, 708 (2005); <https://doi.org/10.1080/10473289.2005.10464656>
- V.P. Aswathi, S. Meera, C.G.A. Maria and M. Nidhin, *Nanotechnol. Environ. Eng.*, **8**, 377 (2023); <https://doi.org/10.1007/s41204-022-00276-8>
- P. Raveendran, J. Fu and S.L. Wallen, *J. Am. Chem. Soc.*, **125**, 13940 (2003); <https://doi.org/10.1021/ja029267j>
- T. Jiao, H. Zhao, J. Zhou, Q. Zhang, X. Luo, J. Hu, Q. Peng and X. Yan, *ACS Sustain. Chem. Eng.*, **3**, 3130 (2015); <https://doi.org/10.1021/acssuschemeng.5b00695>
- K. Li, T. Jiao, R. Xing, G. Zou, J. Zhou, L. Zhang and Q. Peng, *Sci. China Mater.*, **61**, 728 (2018); <https://doi.org/10.1007/s40843-017-9196-8>
- H. Yang, S.J. Bradley, X. Wu, A. Chan, G.I.N. Waterhouse, T. Nann, J. Zhang, P.E. Kruger, S. Ma and S.G. Telfer, *ACS Nano*, **12**, 4594 (2018); <https://doi.org/10.1021/acsnano.8b01022>
- F. Zhan, R. Wang, J. Yin, Z. Han, L. Zhang, T. Jiao, J. Zhou, L. Zhang and Q. Peng, *RSC Adv.*, **9**, 878 (2019); <https://doi.org/10.1039/C8RA08516A>
- L. Ge, M. Zhang, R. Wang, N. Li, L. Zhang, S. Liu and T. Jiao, *RSC Adv.*, **10**, 15091 (2020); <https://doi.org/10.1039/D0RA01884H>
- R. Costi, A.E. Saunders and U. Banin, *Angew. Chem. Int. Ed.*, **49**, 4878 (2010); <https://doi.org/10.1002/anie.200906010>
- Y. Orooji, R. Mohassel, O. Amiri, A. Sobhani and M. Salavati-Niasari, *J. Alloys Compd.*, **835**, 155240 (2020); <https://doi.org/10.1016/j.jallcom.2020.155240>
- Z. Taherian, A. Khataee and Y. Orooji, *Renew. Sustain. Energy Rev.*, **134**, 110130 (2020); <https://doi.org/10.1016/j.rser.2020.110130>
- H. Karimi-Maleh, F. Karimi, Y. Orooji, G. Mansouri, A. Razmjou, A. Aygun and F. Sen, *Sci. Rep.*, **10**, 11699 (2020); <https://doi.org/10.1038/s41598-020-68663-2>

18. M.-B. Gholivand, A.R. Jalalvand, H.C. Goicoechea, G. Paimard and T. Skov, *Talanta*, **131**, 249 (2015); <https://doi.org/10.1016/j.talanta.2014.07.040>
19. R. Hassandoost, S.R. Pouran, A. Khataee, Y. Orooji and S.W. Joo, *J. Hazard. Mater.*, **376**, 200 (2019); <https://doi.org/10.1016/j.jhazmat.2019.05.035>
20. Y. Orooji, M. Ghanbari, O. Amiri and M. Salavati-Niasari, *J. Hazard. Mater.*, **389**, 122079 (2020); <https://doi.org/10.1016/j.jhazmat.2020.122079>
21. J. Perelaer, P.J. Smith, D. Soltman, S.K. Volkman, V. Subramanian, D. Mager, J.G. Korvink and U.S. Schubert, *J. Mater. Chem.*, **20**, 8446 (2010); <https://doi.org/10.1039/c0jm00264j>
22. J. Gao, H. Gu and B. Xu, *Acc. Chem. Res.*, **42**, 1097 (2009); <https://doi.org/10.1021/ar9000026>
23. Y. Wang, A.V. Biradar, G. Wang, K.K. Sharma, C.T. Duncan, S. Rangan and T. Asefa, *Chem. Eur. J.*, **16**, 10735 (2010); <https://doi.org/10.1002/chem.201000354>
24. S. Jeong, H.C. Song, W.W. Lee, S.S. Lee, Y. Choi, W. Son, E.D. Kim, C.H. Paik, S.H. Oh and B.-H. Ryu, *Langmuir*, **27**, 3144 (2011); <https://doi.org/10.1021/la104136w>
25. N. Cioffi, L. Torsi, N. Ditaranto, G. Tantillo, L. Ghibelli, L. Sabbatini, T. Bleve-Zacheo, M. D'Alessio, P.G. Zamboni and E. Traversa, *Chem. Mater.*, **17**, 5255 (2005); <https://doi.org/10.1021/cm0505244>
26. T.M.D. Dang, T.T.T. Le, E. Fribourg-Blanc and M.C. Dang, *Adv. Nat. Sci.: Nanosci. Nanotechnol.*, **2**, 015009 (2011); <https://doi.org/10.1088/2043-6262/2/1/015009>
27. J. Xiong, Y. Wang, Q. Xue and X. Wu, *Green Chem.*, **13**, 900 (2011); <https://doi.org/10.1039/c0gc00772b>
28. R. Sankar, P. Manikandan, V. Malarvizhi, T. Fathima, K.S. Shivashangari and V. Ravikumar, *Spectrochim. Acta A Mol. Biomol. Spectrosc.*, **121**, 746 (2014); <https://doi.org/10.1016/j.saa.2013.12.020>
29. S. Yallappa, J. Manjanna, M.A. Sindhe, N.D. Satyanarayan, S.N. Pramod and K. Nagaraja, *Spectrochim. Acta A Mol. Biomol. Spectrosc.*, **110**, 108 (2013); <https://doi.org/10.1016/j.saa.2013.03.005>
30. R. Srivastava, *Pharmacogn. Rev.*, **8**, 36 (2014); <https://doi.org/10.4103/0973-7847.125528>
31. J. Fick, H. Söderström, R.H. Lindberg, C. Phan, M. Tysklind and D.G.J. Larsson, *Environ. Toxicol. Chem.*, **28**, 2522 (2009); <https://doi.org/10.1897/09-073.1>
32. P. Deka, D. Bhattacharjee, P. Sarmah, R.C. Deka and P. Bharali, in eds.: F. Kurisu, A. Ramanathan, A. Kazmi and M. Kumar, Catalytic Reduction of Water Contaminant '4-Nitrophenol' over Manganese Oxide Supported Ni Nanoparticles; In: Trends in Asian Water Environmental Science and Technology, Springer International Publishing, Cham, pp. 35-48 (2017).
33. T. Achamo and O.P. Yadav, *Anal. Chem. Insights*, **11**, S31508 (2016); <https://doi.org/10.4137/ACI.S31508>
34. R.D. Neal, Y. Inoue, R.A. Hughes and S. Neretina, *J. Phys. Chem. C*, **123**, 12894 (2019); <https://doi.org/10.1021/acs.jpcc.9b02396>
35. J. Zhang, G. Chen, D. Guay, M. Chaker and D. Ma, *Nanoscale*, **6**, 2125 (2014); <https://doi.org/10.1039/C3NR04715F>
36. Y. Woo and D.Y. Lai, Aromatic Amino and Nitro-Amino Compounds and Their Halogenated Derivatives, in Patten's Toxicology, Wiley, pp. 1-96 (2012).
37. N.F. Abd Razak and M. Shamsuddin, *Inorg. Nano-Met. Chem.*, **50**, 489 (2020); <https://doi.org/10.1080/24701556.2020.1720724>
38. N.K.R. Bogireddy, P. Sahare, U. Pal, S.F.O. Méndez, L.M. Gomez and V. Agarwal, *Chem. Eng. J.*, **388**, 124237 (2020); <https://doi.org/10.1016/j.cej.2020.124237>
39. W. Shen, Y. Qu, X. Pei, S. Li, S. You, J. Wang, Z. Zhang and J. Zhou, *J. Hazard. Mater.*, **321**, 299 (2017); <https://doi.org/10.1016/j.jhazmat.2016.07.051>
40. Z. Xiong, H. Zhang, W. Zhang, B. Lai and G. Yao, *Chem. Eng. J.*, **359**, 13 (2019); <https://doi.org/10.1016/j.cej.2018.11.111>
41. P. Zhao, X. Feng, D. Huang, G. Yang and D. Astruc, *Coord. Chem. Rev.*, **287**, 114 (2015); <https://doi.org/10.1016/j.ccr.2015.01.002>
42. Z. Yan, N. Wang, M. Zhang, M. Xiang and Z. Xu, *J. Environ. Chem. Eng.*, **9**, 106174 (2021); <https://doi.org/10.1016/j.jece.2021.106174>
43. A. Ahmad, Y. Wei, F. Syed, S. Khan, G.M. Khan, K. Tahir, A.U. Khan, M. Raza, F.U. Khan and Q. Yuan, *J. Photochem. Photobiol. B*, **161**, 17 (2016); <https://doi.org/10.1016/j.jphotobiol.2016.05.003>
44. S.A. Prisin, M. Priyanga, K.M. Ponvel, K. Kaviarasan and S. Kalidass, *J. Cluster Sci.*, **33**, 765 (2022); <https://doi.org/10.1007/s10876-021-02016-5>
45. S. Kumar, S. Baruah and A. Puzari, *Polym. Bull.*, **77**, 441 (2020); <https://doi.org/10.1007/s00289-019-02760-9>
46. N.Y. Baran, T. Baran and M. Nasrollahzadeh, *Sci. Rep.*, **13**, 12008 (2023); <https://doi.org/10.1038/s41598-023-38898-w>
47. Z. Liu, B. Hu, D. Li, P. Zhu, Y. Ye and R. Shen, *Appl. Phys.*, **72**, 30401 (2015).
48. Y. Keereeta, R. Sirirak and A. Klinbumrung, *Micro and Nanostructures*, **186**, 207757 (2024); <https://doi.org/10.1016/j.micrna.2024.207757>
49. M. Tranchant, A. Serrà, C. Gunderson, E. Bertero, J. García-Amorós, E. Gómez, J. Michler and L. Philippe, *Appl. Catal. A Gen.*, **602**, 117698 (2020); <https://doi.org/10.1016/j.apcata.2020.117698>
50. M. Sivagami and I.V. Asharani, *J. Taiwan Inst. Chem. Eng.*, **149**, 104981 (2023); <https://doi.org/10.1016/j.jtice.2023.104981>